Daily reservoir inflow forecasting using weather forecast downscaling and rainfall-runoff modeling

Application to Urmia Lake basin, Iran

Meydani, Amirreza; Dehghanipour, Amirhossein; Schoups, Gerrit; Tajrishy, Massoud

DOI
10.1016/j.ejrh.2022.101228

Publication date
2022

Document Version
Final published version

Published in
Journal of Hydrology: Regional Studies

Citation (APA)
Meydani, A., Dehghanipour, A., Schoups, G., & Tajrishy, M. (2022). Daily reservoir inflow forecasting using weather forecast downscaling and rainfall-runoff modeling: Application to Urmia Lake basin, Iran. *Journal of Hydrology: Regional Studies*, *44*, Article 101228. https://doi.org/10.1016/j.ejrh.2022.101228

Journal of Hydrology: Regional Studies 44 (2022) 101228

Contents lists available at ScienceDirect

Journal of Hydrology: Regional Studies

journal homepage: www.elsevier.com/locate/ejrh

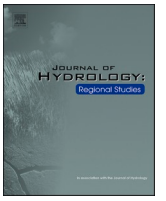

Daily reservoir inflow forecasting using weather forecast downscaling and rainfall-runoff modeling: Application to Urmia Lake basin, Iran

Amirreza Meydani [a,b], Amirhossein Dehghanipour [c], Gerrit Schoups [c,*], Massoud Tajrishy [a]

[a] Department of Civil Engineering, Sharif University of Technology, Tehran, Iran
[b] Department of Geography and Spatial Sciences, University of Delaware, Newark, DE, USA
[c] Department of Water Management, Faculty of Civil Engineering and Geosciences, Delft University of Technology, Delft, the Netherlands

ARTICLE INFO

Keywords:
Downscaling
ECMWF
NCEP
Runoff Forecast System
Urmia Lake
Bukan reservoir

ABSTRACT

Study region: This study develops the first daily runoff forecast system for Bukan reservoir in Urmia Lake basin (ULB), Iran, a region suffering from water shortages and competing water demands.
Study focus: A weather forecast downscaling model is developed for downscaling large-scale raw weather forecasts of ECMWF and NCEP to small-scale spatial resolutions. Various downscaling methods are compared, including deterministic Artificial Intelligence (AI) techniques and a Bayesian Belief Network (BBN). Downscaled precipitation and temperature forecasts are then fed into a rainfall-runoff model that accounts for daily snow and soil moisture dynamics in the sub-basins upstream of Bukan reservoir. The multi-objective Particle Swarm Optimization (MOPSO) method is used to estimate hydrological model parameters by maximizing the simulation accuracy of observed river flow (NSE_Q) and the logarithm of river flow (NSE_{LogQ}) in each sub-basin.
New hydrological insights for the region: Results of the weather forecast downscaling model show that the accuracy of the BBN is greater than the various deterministic AI methods tested. Calibration results of the rainfall-runoff model indicate no significant trade-off between fitting daily high and low flows, with an average NSE_Q and NSE_{LogQ} of 0.43 and 0.63 for the calibration period, and 0.54 and 0.57 for the validation period. The entire forecasting system was evaluated using inflow observations for years 2020 and 2021, resulting in an NSE of 0.66 for forecasting daily inflow into Bukan reservoir. The inflow forecasts can be used by policymakers and operators of the reservoir to optimize water allocation between agricultural and environmental demands in the ULB.

1. Introduction

Increased agricultural water consumption along with repercussions of climate change, drought, and mismanagement of water resources leads to competition for water supply between agriculture and environmental sectors and has brought adverse

* Correspondence to: Faculty of Civil Engineering and Geosciences, Delft University of Technology, Delft, the Netherlands.
E-mail addresses: meydani@udel.edu (A. Meydani), a.dehghanipour@tudelft.nl (A. Dehghanipour), g.h.w.schoups@tudelft.nl (G. Schoups), tajrishy@sharif.edu (M. Tajrishy).

https://doi.org/10.1016/j.ejrh.2022.101228
Received 17 February 2022; Received in revised form 12 August 2022; Accepted 3 October 2022
Available online 8 October 2022

environmental effects such as the destruction of ecosystems and natural bodies of water, especially in arid and semi-arid regions (Dehghanipour et al., 2020; Dunn et al., 2003; Khorasani et al., 2018; Mancosu et al., 2015; Sisto, 2009; Valipour et al., 2015; Xue et al., 2017). Seasonal weather forecast models can be an invaluable tool to manage competing water demands from agriculture and the environment (Rayner et al., 2005). Seasonal weather forecast models enable water resources managers to adapt their actions to pre-emptively resolve any shortages or decide optimal planning. Applying weather forecasts in water resources management leads to better foresight of water-related risks (Grillakis et al., 2018) and increases sustainability in agriculture and natural ecosystems. Several studies accounted for using weather forecasts in flood management (Voisin et al., 2011; Wang et al., 2012), multi-reservoir operation (Ficchì et al., 2016), and optimal agricultural water allocation (Kaune et al., 2020).

The European Center for Medium Range Weather Forecast (ECMWF) and the National Center for Environmental Prediction (NCEP), provide real-time and seasonal weather forecasts. Various studies have evaluated ECMWF seasonal forecast capabilities, including its temperature forecast performance over South America (Gubler et al., 2020), precipitation performance over central Himalaya (Chen et al., 2021), temperature and precipitation skills in the Danube basin (Voisin et al., 2011), and prediction of Caspian sea level (Arpe et al., 2014). The NCEP forecasts showed good performance in various studies for precipitation and temperature forecasting (Phan-Van et al., 2018; Sangelantoni et al., 2019; Yuan et al., 2013) and drought prediction (Lang et al., 2020).

These forecasts usually have a coarse spatial resolution, limiting their direct use in regional-scale applications (Siegmund et al., 2015). Therefore, a downscaling method should be applied to convert the forecasts for regional-scale applications. In this regard, several studies have applied AI in developing precipitation (Kisi and Cimen, 2012), temperature (Chevalier et al., 2011), evaporation (Dehghanipour et al., 2021), and runoff (Adamowski, 2013; Munoz et al., 2021) forecast models using observed historical data (Liu et al., 2021). However, using observational data to forecast future precipitation increases uncertainty because precipitation is a random phenomenon requiring the use of complex dynamics and numerical procedures to be forecast (ECMWF, 2013). Hybrid AI models combine several methods that can reduce uncertainty (Ahmadi et al., 2019). However, few studies have applied hybrid AI for downscaling seasonal weather forecasts (Sun and Lan, 2021).

In addition to using deterministic AI methods, probabilistic models such as BBNs have been applied for estimating weather variables such as precipitation (Hruschka and Nicoletti, 2013). While BBNs are an appropriate approach in situations with high uncertainty and complexity (Molina et al., 2013), no study has used this method to downscale seasonal weather forecasts.

In this study, we focus on weather and runoff forecasting in the ULB. Bukan reservoir is the largest reservoir in ULB, and is located upstream of the Zarrineh Rood River (ZRR). Recent research investigated the long-term climate change effects on water resources in the ZRR basin and indicated a decrease in precipitation upstream of ZRR, leading to a decline in runoff to Bukan reservoir in the future (Dariane and Pouryafar, 2021). In the face of reducing precipitation and increasing agricultural water consumption in ULB, the development of a runoff forecast system for this reservoir can help policymakers optimize water allocation between agricultural and environmental sectors in ULB.

While there have been numerous modeling studies in ULB, runoff forecasting has received little attention, with past studies focusing on either simulating historical hydrological dynamics (Dehghanipour et al., 2020, 2019) or developing long-term scenarios and projections for the distant future (Emami and Koch, 2019; Mahmudi et al., 2021). Moreover, the simulation of snow accumulation and river runoff in sub-basins upstream of Bukan reservoir has only been done on a monthly scale so far (Ahmadaali et al., 2017; Mostafazade and Alizadeh, 2020). Finally, a model that can forecast future water balance components using real-time weather forecasts data has not been proposed for the region because most studies used observed historical data instead of forecast runoff (Gavahi et al., 2019).

In this study, a weather forecast downscaling model is coupled to a daily hydrological rainfall-runoff model to forecast inflow into Bukan reservoir. The resulting runoff and inflow forecasts support water resources management plans to increase the inflow to Urmia lake (UL) and reduce the impacts of both water scarcity and flooding. This research has the following innovations compared to previous studies. First, a weather forecast downscaling model is developed, comparing hybrid deterministic AI and probabilistic BBN methods for downscaling the raw ECMWF and NCEP weather forecasts. Second, an existing rainfall-runoff model is implemented for the first time in this region for modeling daily snow and soil moisture dynamics with a two-storage method that accounts for snow accumulation and melt, actual evapotranspiration, irrigation, surface and subsurface runoff, and groundwater recharge. In contrast, previous studies have only considered monthly dynamics resulting in a less accurate simulation of water balance components. Third, although some research has developed a rainfall-runoff model for this region, these models (e.g., SWAT) are complex and require many input data and calibration parameters. Since the required data of these models are not available in the study area, simplifying assumptions were used to estimate the required data and parameters of the model, leading to errors and uncertainties in river runoff simulation. However, our method uses fewer input data collected in the region leading to no simplifying assumptions, and at the same time, the complexity of the model improves its performance and maintains the capabilities of previous models.

The paper is divided into five sections. Section 2 introduces the study area. Section 3 describes the methodology, including developing the weather forecast model, the downscaling methods, the hydrological rainfall-runoff model, and the calibration approach. Results and discussion are presented in Section 4, and the conclusions are presented in Section 5.

2. Study area

ULB, with an approximate area of 51,760 km^2, is one of the largest endorheic basins in Iran, located in the mountainous region of northwestern Iran. UL is located in the center of ULB, and it is a drainage place of the whole basin's surface water. The surface water supply of UL originates from six important rivers: ZRR, Simineh Rood, Ajichay, Ghadarchay, Shahrchay, and Zolachay (Fig. 1a).

ZRR is the largest and most important river in UL. The average annual runoff of this river is about 2000 MCM, and it supplies more

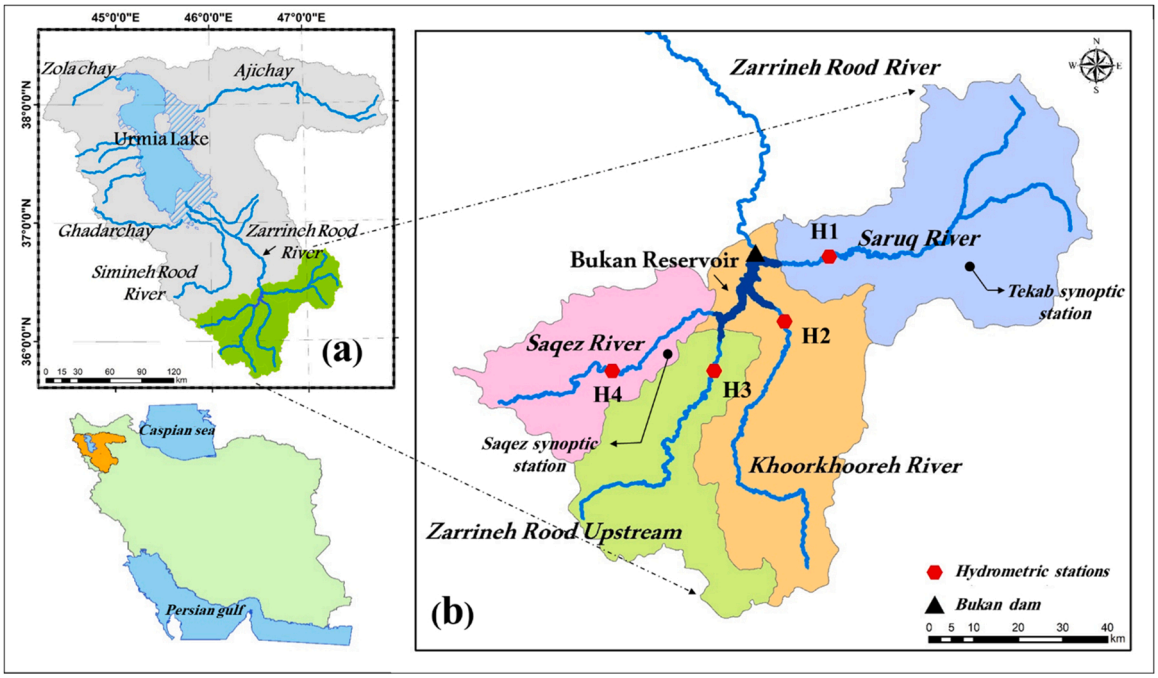

Fig. 1. Location of the study area (a) Bukan reservoir and its main upstream rivers in ULB, Iran; and (b) Sub-basins in upstream Bukan reservoir (See the names of hydrometric stations (H1, H2, H3, and H4) in Table 5).

than 40 % of the total annual environmental flow to UL (Ghaheri et al., 1999; Meydani et al., 2021). Moreover, Bukan reservoir, as the biggest reservoir in the ULB, is located on the ZRR (Dehghanipour et al., 2020, 2019).

In this study, four sub-basins of the ZRR basin located upstream of Bukan reservoir are selected as a case study (Fig. 1). The sub-basins include Saqez River, ZRR upstream, Khoorkhooreh River, and Saruq River. The mean annual precipitation and temperature are about 650 mm and 10 °C, respectively, for these sub-basins (Yekom Consulting Engineers, 2016). Most of the precipitation from mid-December to early March is snow (Fig. 2), and the average snow area is 53 % of the total area (Yekom Consulting Engineers, 2016). Therefore, snow is one of this region's primary water balance components, and the flow regime in these sub-basins is snow-rainy (Yekom Consulting Engineers, 2016). Snowmelt accounts for about 67 % of annual runoff. There are no significant aquifers in the region.

Bukan reservoir was built in 1971 with a storage capacity of 650 MCM, which was increased to 808 MCM in 2005. Saruq, Khoorkhooreh, and Saqez rivers are tributaries of the ZRR and supply additional inflow into Bukan reservoir (Fig. 1b). Bukan reservoir provides drinking water for major cities such as Tabriz, Bukan, and Miyandoab, and it is also a strategic surface water source for irrigated agriculture in Sain Qaleh and Miyandoab plains downstream of the reservoir. Sain Qaleh and Miyandoab plains, with an approximate area of 17,000 ha and 100,000 ha, are the most modern and most extensive agricultural irrigated plains of this basin, and about 64% of the rural employment is in the agricultural sector (Dehghanipour et al., 2020). The net annual releases from Bukan reservoir amount to 500 and 80 MCM of water to meet agricultural and urban water demands in Miyandoab and Sain Qala plains, respectively (Yekom Consulting Engineers, 2016).

3. Methodology

In this study, a runoff forecast model was developed to forecast inflow to Bukan reservoir, an essential and strategic reservoir in ULB. The runoff forecast model helps policymakers optimize allocation to agricultural demands, drinking water, and environmental requirements downstream of Bukan reservoir. As outlined in Fig. 3, this model consists of (1) a weather forecast downscaling model and (2) a hydrological rainfall-runoff model. Meteorological input data for the models were based on observed data from Tekab synoptic station for the Saruq river sub-basin, and from Saqez synoptic station for the other sub-basins (Fig. 1). These two stations were chosen because they have high-quality data and little missing data during the modeling period.

The weather forecast downscaling model was developed to downscale large-scale raw weather forecast data of ECMWF and NCEP to small-scale resolutions. The downscaling procedure helps to reduce errors between observed data and the nearest grid point. The forecasted weather variables include monthly precipitation and daily temperature. Since the rainfall-runoff model has a daily time scale, the monthly forecasted precipitation was disaggregated to daily forecasted precipitation based on the daily distribution of raw forecast data in each month. The spatially downscaled and temporally disaggregated precipitation and temperature data are subsequently used as inputs to the hydrological rainfall-runoff model. The hydrological rainfall-runoff model simulates water balance

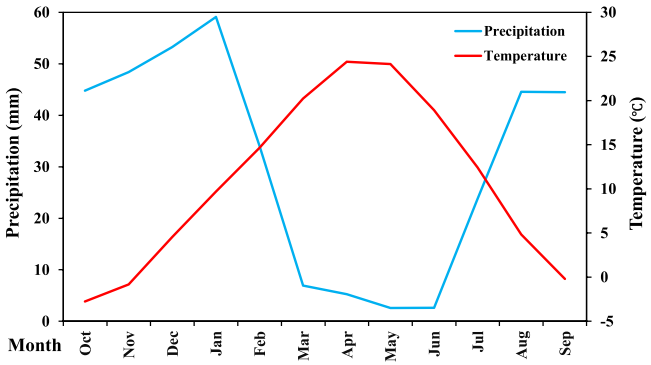

Fig. 2. Ombrothermic diagram for sub-basins in upstream Bukan reservoir using monthly time-averaged observed precipitation and temperature data for the period 1995–2020.
Source: Saqez and Tekab stations, Iran Meteorological Organization, see https://data.irimo.ir/.

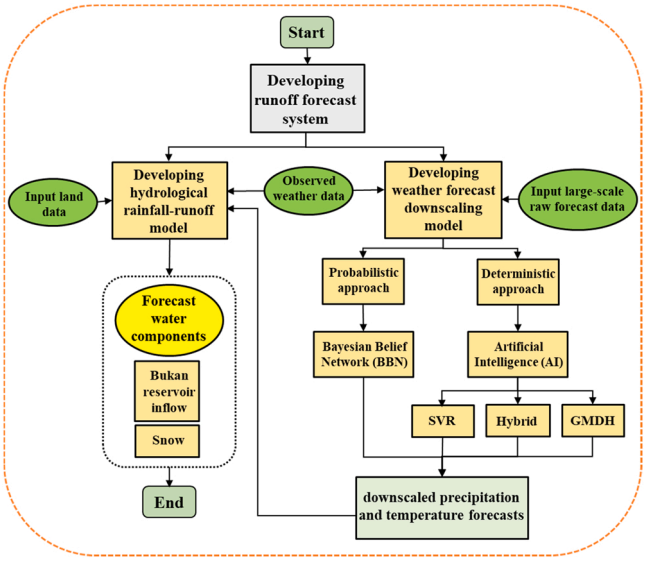

Fig. 3. Outline of the developed runoff forecast system including integrated weather forecast downscaling model and hydrological rainfall-runoff model.

components, including snow storage, snowmelt, actual evapotranspiration, surface runoff, and subsurface flow for sub-basins upstream of Bukan reservoir. The output of the hydrological rainfall-runoff model consists of daily forecasted inflow to Bukan reservoir at the beginning of each month and for a 1-month lead time. In the following sections, we discuss the various parts of both models in more detail. Furthermore, more details are provided in Table 1 about the periods and input data used in each model.

Table 1
Summary of the calibration and validation process for weather forecast downscaling and hydrological rainfall-runoff models.

Model		Data	Time scale	Calibration period (Train)	Validation period (Test)	Forecast period
Weather forecast downscaling	Temperature	ECMWF and NCEP's temperature and observed temperature	Daily	2010–2017	2017–2019	2019–2021
	Precipitation	ECMWF and NCEP's precipitation, Month number, and observed precipitation	Monthly			
Hydrological rainfall-runoff		Observed weather data and observed river discharge	Daily	2003–2014	1999–2003	

3.1. Weather forecast downscaling model

3.1.1. ECMWF forecasts

ECMWF is run by an independent intergovernmental entity supported by 34 European nations. These forecasts are based on mathematical models of the atmosphere and oceans to forecast weather variables based on current and initial weather conditions. Therefore, different meteorological organizations operate different models for forecasting atmospheric conditions, and the results vary for the same area. The ECMWF system has been upgraded every five years, with SEAS5 the fifth and latest seasonal forecast system (Johnson et al., 2019). Seasonal forecasts are possible due to the slow evolution of some of the earth's components and their effect on the atmosphere. The seasonal forecasts provide information on the upcoming season's weather conditions and are useful for various sectors, such as water resources management, agriculture, health, and energy (ECMWF, 2013). Here, we use SEAS5. ECMWF provides seasonal forecast data from 1993 to 2016 as hindcast data calibrated and verified using a set of retrospective seasonal forecasts for past dates and is more accurate compared to the historical data (Johnson et al., 2019). From 2017 onward, forecast instead of hindcast data is available. In this study, the ensemble mean of seasonal monthly and daily weather forecast data, i.e., respectively "Seasonal forecast monthly statistics on the single level" and "Seasonal forecast daily and sub-daily data on the single level", were downloaded (ECMWF, 2021a,b). These global products have a horizontal resolution of 1 degree. The lowest monthly precipitation lead time, i.e. 1-month lead time, was selected for downscaling to have more accurate forecasts. It should be noted that initially, the daily precipitation data were downscaled, while the results were not satisfactory because precipitation is a highly uncertain phenomenon, so monthly precipitation downscaling was considered as the main objective of this study. Daily temperature data were downscaled with a 6-month lead time because temperature forecasts are much less uncertain than precipitation.

3.1.2. NCEP forecasts

The US Government runs NCEP under the leadership of the National Oceanic and Atmospheric Administration and its subsidiary agencies. The second version of the Climate Forecast System (CFSv2) became operational in 2011. CFSv2 has higher skill than version 1, due to improvements in the initial state of its underlying model (Saha et al., 2014). Data used in this study are from the "CFSv2 operational forecasts time series" product and monthly precipitation and temperature, and daily temperature. In this study, to prevent confusion and easy understanding of results, GFSv2's products are called NCEP. For NCEP, precipitation and temperature forecasts were downloaded for 1-month and 6-month lead times, respectively (NCEP, 2011).

3.1.3. AI downscaling methods

The meteorological models used in this study are global and large-scale. The outputs of meteorological models need to be downscaled to small-scale resolutions in the study region to reduce forecast errors. Recently, AI has been used for downscaling weather forecasts due to its ability to identify complex patterns and unforeseen behavior (Benderskaya, 2013), and its capability of extracting non-linear relations from data without prior knowledge of the parametric form of these relations (Valverde Ramírez et al., 2006). Here, we downscale the forecasts to the point-scale of synoptic weather stations, whose data are used to force the hydrological rainfall-runoff model. In this study, three AI methods are used for downscaling raw weather forecast data, as detailed below. Each method contains parameters that are estimated by minimizing the discrepancy between the downscaled precipitation and temperature estimates and their weather-station observed counterparts, with discrepancy quantified by Eq. 1. In addition to NSE, the RMSE criterion is used to quantify performance of the downscaled forecasts:

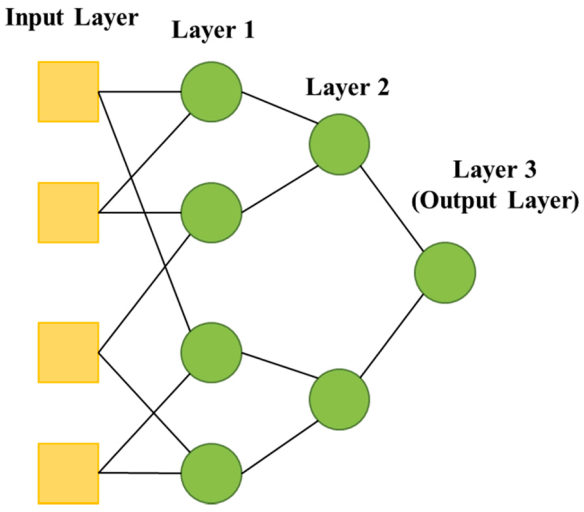

Fig. 4. Structure of GMDH neural network with four inputs.

$$NSE = 1 - \frac{\sum_{i=1}^{m}\left(V_{obs}^{i} - V_{down}^{i}\right)^2}{\sum_{i=1}^{m}\left(V_{obs}^{i} - \bar{V}_{obs}\right)^2} \tag{1}$$

$$RMSE = \sqrt{\sum_{i=1}^{m}\frac{\left(V_{down}^{i} - V_{obs}^{i}\right)^2}{m}} \tag{2}$$

where, V_{obs}^{i} and V_{down}^{i} are observed data and downscaled forecasts, respectively, at the synoptic station. Furthermore, the ratio of the train data to the test data was 70–30. More information on three methods is presented in the following sections.

3.1.3.1. Group method of data handling (GMDH). The first method is based on a multilayer network, where each layer acts as a non-linear function of its inputs (Ivakhnenko, 1970). Input data define the number of neurons. For instance, if the number of input variables is k, the number of neurons in each layer equals $m = \binom{k}{2}$, which will enter the neuron as a binary permutation. Fig. 4 shows the multilayer structure of the GMDH neural network model.

The main objective of this method is to define a function that minimizes the difference between downscaled forecast data and observed data of synoptic stations. At first, as one of the best polynomial equations (Eq. 3), Volterra equation was applied to construct a high order polynomial by (Ivakhnenko, 1970). Generally, Eq. 3 is used to calculate up to the square terms as Eq. 4 to determine the correlation between raw forecast data and observed gauge data.

$$y = a_0 + \sum_{i=1}^{n} a_i x_i + \sum_{i=1}^{n}\sum_{j=1}^{n} a_{ij} x_i x_j + \sum_{i=1}^{n}\sum_{j=1}^{n}\sum_{k=1}^{n} a_{ijk} x_i x_j x_k + \ldots \tag{3}$$

$$y = a_0 + \sum_{i=1}^{n} a_i x_i + \sum_{i=1}^{n}\sum_{j=1}^{n} a_{ij} x_i x_j \tag{4}$$

where, a_0, a_i, a_{ij} are coefficients of variables in the polynomial that can be calculated by the least squares error method, x_i,x_j,$x_k$are input variables which are combined pairwise in each neuron based on Eq. 4, and n is the number of variables in each combination (n = 2). This method considers all pairwise combinations in a time series, and each combination is fed to each neuron in Fig. 4. In other words, the coefficients of Eq. 4 are estimated in each neuron, and the output is calculated using input variables. Then, the NSE values between model output and data of each neuron are calculated, and neurons are sorted based on NSE values in order to eliminate deficient neurons step by step (Nariman-zadeh et al., 2002). Inputs to the GMDH model for downscaling precipitation are a combination of raw forecast data of precipitation at time step t and t-*1*, the month number and precipitation of observed gauge data in time step t. Raw forecast and observed gauge data of temperature are input variables to downscaling temperature. Selected neurons are the inputs to the next layer. The process is continued until the last layer in which the obtained neuron is the estimated a_0, a_i, a_{ij} for the time series.

3.1.3.2. Support vector regression (SVR). The idea of SVR is to approximate the best value within the margin called ε-sensitive zone by minimizing the error inside a specific threshold like Fig. 5 for a linear function. Due to the non-linear nature of the problem, with the help of SVR, regression function in the form of Eq. 5 is obtained.

$$f(x) = w\phi(x) + b \tag{5}$$

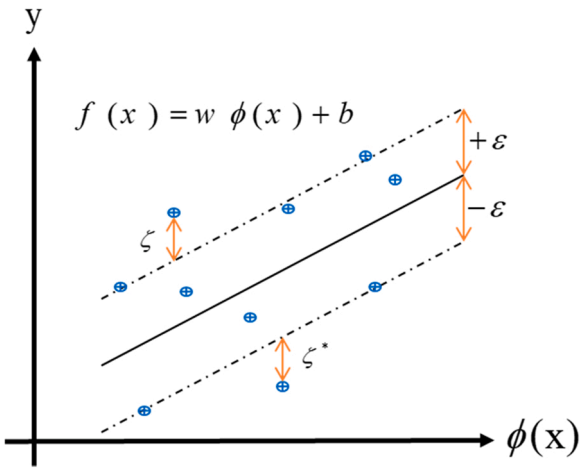

Fig. 5. The best approximation value ε to minimize the error in a specific threshold corresponds to SVR.

where $\phi(x)$ is a non-linear transfer function to map raw forecast data to higher dimensional space. w is a weight factor, and b is a deviation constant.

In Fig. 5, the straight line is the hyperplane that separates the line between two classes in a higher dimension than the actual dimension. The dashed line in Fig. 5 shows the boundaries at a distance ε to create a margin between, for example, raw precipitation forecast data. Indeed, ε represents the quality of optimization and states deviation between observed gauge data and downscaled forecast data. With the help of risk minimization (Eq. 6), Eq. 5 is solved at a higher dimension for raw forecast data to make linear separation possible.

$$R\left(w,\zeta,\zeta^{*}\right)=\frac{1}{2}\|w\|^{2}+C\sum_{i=1}^{m}\left(\zeta_{i}+\zeta_{i}^{*}\right)$$

$$\text{subject to}:\begin{cases} y_{i}-\left(w\phi(x_{i})+b_{i}\right)\le\varepsilon+\zeta_{i} \\ \left(w\phi(x_{i})+b_{i}\right)-y_{i}\le\varepsilon+\zeta_{i}^{*} \\ \zeta_{i}^{*},\zeta_{i}\ge 0 \end{cases} \tag{6}$$

where, x and y are raw and downscaled forecast data, respectively. In the above equations, given the training sample set (x_i,y_i), x_i is the n-dimensional input vector for different variables mentioned in GMDH method and y_i is the desired 1-dimensional output at the point i, $x_i\in R^n$, $y_i\in R^n$. ζ,ζ^{*} are slack variables to measure errors for any variable that falls outside of ε in upside and downside, respectively. $b\in R^n$ and $w\in R^n$ are constants for showing deviation and weight factor, respectively, and C is a regularization constant for balancing error minimization and maximization. m is the size of raw forecast data, $f(x)$ is the modeled target that calculates downscaled forecast data based on the observed gauge data (Dodangeh et al., 2020). Using the Lagrange function method, Non-linear regression becomes Eq. 7, where Kernel function is used to transform data into higher dimension space (for more detail about Lagrange and Kernel transformations, see (Geng et al., 2020; Yaghoubi et al., 2019).

$$f(x)=\sum_{i=1}^{m}\left(\alpha_{i}+\alpha_{i}^{*}\right)k\left(x,x_{i}\right)+b \tag{7}$$

where $k(x,x_i)=(\phi(x),\phi(x_i))$ is Kernel function, a Gaussian type of Kernel equation is used in this study, and α_i,α_i^{*} are Lagrange coefficients. NSE function (Eq. 1) is used between downscaled forecast and observed gauge data to optimize model parameters, including C,ε, and Kernel function parameters.

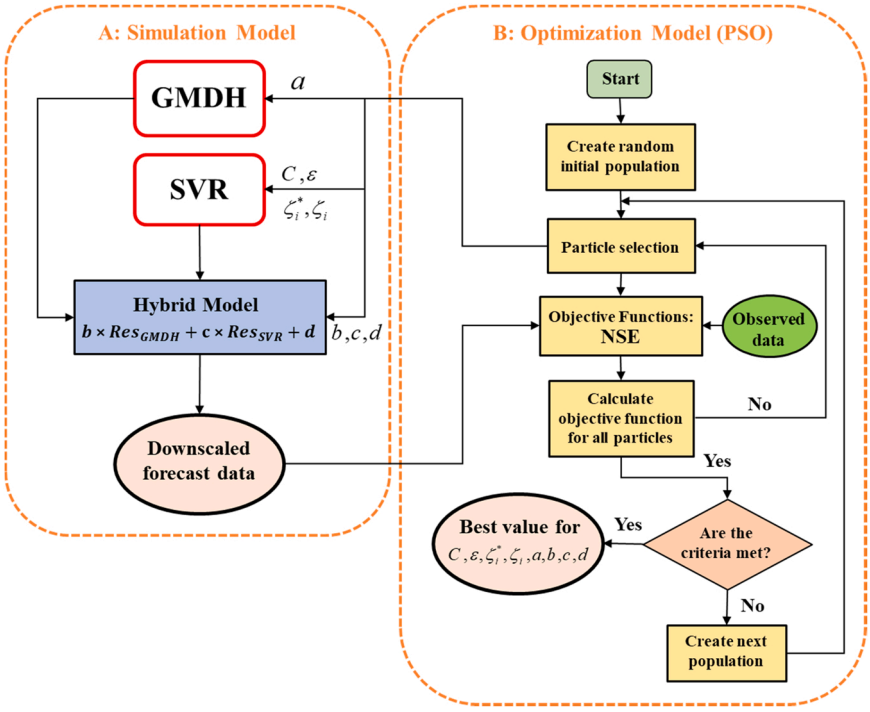

Fig. 6. A hybrid SVR-GMDH model for downscaling precipitation data. The parameters of hybrid model are optimized by PSO.

3.1.3.3. Hybrid AI downscaling method (SVR-GMDH). We also test a hybrid approach that combines GMDH and SVR (Fig. 6). Applying the GMDH and SVR forms an efficient downscaling model because of GMDH's capability in modeling highly non-linear relations, and SVR's independence on the dimensionality of the input space due to its model computational complexity (Dodangeh et al., 2020). In this case, raw precipitation forecast data are used to produce downscaled estimates with both GMDH and SVR, and the final hybrid downscaled values are then estimated as a linear combination of the GMDH and SVR outputs. Coefficients *b*, *c,* and *d* of the linear combination and coefficients of the individual methods are jointly optimized by Particle Swarm Optimization (PSO) with Eq. 1 as the objective function in order to increase the efficiency.

3.1.4. BBN downscaling method

BBNs were introduced in the late 1980s, and they have been used frequently in water resources planning and management (Govender et al., 2021; Phan et al., 2016; Xue et al., 2017). For instance, BBNs were applied to estimate missing rainfall data (Sun et al., 2017) and forecast flood peaks (Goodarzi et al., 2019). Khan and Coulibaly (2006) reported better performance of a BBN compared to an Artificial Neural Network for simulating daily river flow and reservoir inflow.

The BBN is a probabilistic graphical model consisting of nodes arranged in an acyclic directional graph. Nodes represent discrete or continuous random variables, and the direction of the arrows indicates whether or not the nodes are dependent on each other. The head node of the arrow is called the child node, and the start node is called the parent node so that the child node is dependent on the parent node. A node without parents and a node without children is called the root node and leaf node, respectively. If the nodes represent discrete random variables, then conditional probability tables (CPTs) are used to quantify the probabilistic influence of the parent nodes on the child node.

Values for the entries in the CPTs, where each entry represents the conditional probability of a child node state given its parent node states, are obtained by training or calibrating the BBN using observed gauge precipitation data from synoptic stations. Sensitivity analysis and cross-validation tests are used to validate the model. Validation tests are based on the Confusion matrix, the Accuracy criterion, and the Receiver Operating Characteristic (ROC) Curve (Fawcett, 2006).

The BBN for downscaling monthly precipitation forecasts is shown in Fig. 7. It consists of four nodes, i.e., one child node for downscaled precipitation and three parent nodes representing precipitation forecasts for the previous and current month, as well as the number of the current month. Downscaled precipitation and raw forecast precipitation were classified in two categories to perform probabilistic classification, shown in Table 2. Continuous forecast precipitation values can be obtained by multiplying the probability of each category into the mean of upper and lower limits of Table 2.

3.2. Hydrological rainfall-runoff model

The hydrological rainfall-runoff model was developed using two snow and soil moisture storages illustrated in Fig. 8. The parameters presented in Fig. 8 and their equations are shown in Table 3 and Table 4 for snow and soil moisture storages, respectively. Snow and soil moisture water balance equations are applied for each sub-basin on a daily scale. The input water balance component to the snow storage is precipitation, and its output water balance component is effective precipitation (P_e) (Table 3). In particular, effective precipitation (P_e) enters the soil moisture storage dependent on the air temperature and its comparison with freezing point (T_F) and melting point (T_M) (Fig. 8). The output components of soil moisture storage include actual evapotranspiration (ET_{ac}), irrigation ($Q_{ISW} + Q_{IGW}$), surface runoff (Q_{sur}), subsurface runoff (Q_{int}), and groundwater recharge (Q_r). As shown in Table 4, these output components are calculated by empirical functions based on relative soil water content (Z_1). The value of Z_1 varies between 0 (dry soil) and 1 (saturated soil).

The two-storage model contains six parameters: (1) freezing temperature of snow (T_F), (2) melting temperature of snow (T_M), (3) runoff resistance factor (RRF), (4) root zone conductivity (K), (5) soil water capacity (SWC), and (6) initial soil moisture in the root zone (Z_1). RRF controls surface runoff so that a significant value of RRF causes less surface runoff. This parameter depends on vegetation. Root zone conductivity (K) is a function of soil type, and initial soil moisture in the root zone (Z_1) is the percentage of occupied water ratio to the adequate total root zone storage at the beginning of the simulation.

We consider four sub-basins upstream of Bukan reservoir, corresponding to four rivers, namely ZRR upstream, Saruq river, Khoorkhooreh river, and Saqez river (Fig. 1b). Separate snow and soil moisture storages are considered for each sub-basin. There is no

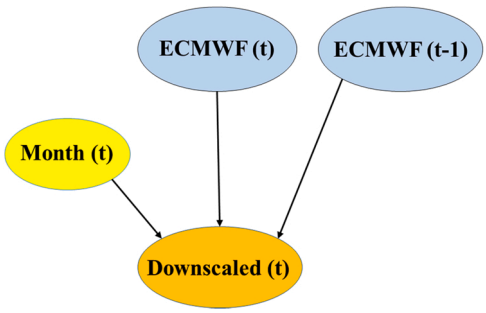

Fig. 7. The schematic of BBN for downscaling precipitation forecast.

Table 2
Classification of CPTs for each node in BBN for downscaling precipitation forecast.

Group	Name	Explanation	States	Time scale
Intervention variables	Month (t)	–	S1(Jan); S2(Feb); S3(Mar); S4(Apr); S5(May); S6(Jun); S7(Jul); S8(Aug); S9(Sep); S10(Oct); S11(Nov); S12(Dec)	Monthly
	ECMWF (t-1)	(mm)	S1(0–0.4); S2(0.4–2); S3(2–9.3); S4(9.3–42.2); S5(42.2–64.2); S6(64.2–85.9); S7	
	ECMWF (t)	(mm)	(85.9–114.2); S8(114.2–186.9)	
Objective variable	Downscaled (t)	(mm)	S1(0–1.3); S2(1.3–14.2); S3(14.2–38.9); S4(38.9–68.6); S5(68.6–189)	

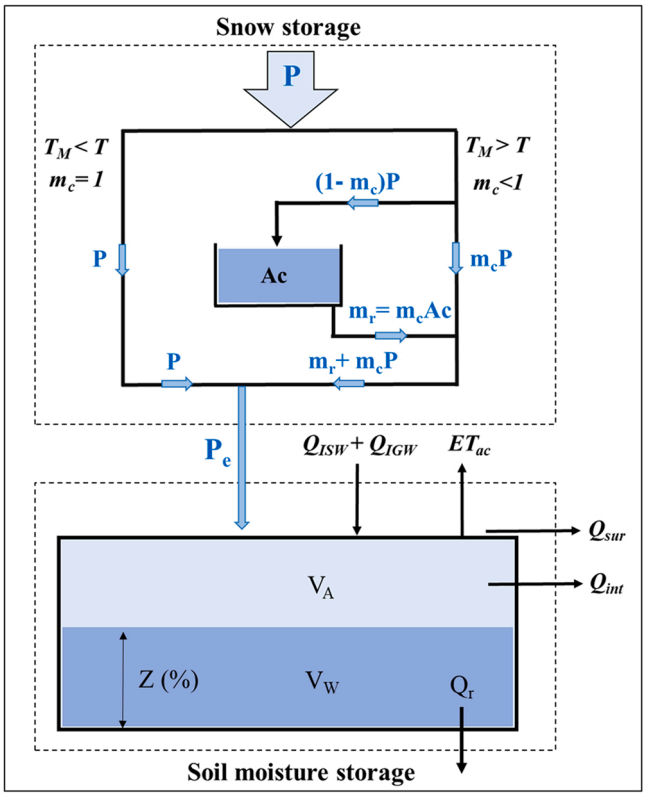

Fig. 8. Schematic diagram of the hydrological rainfall-runoff model consisting of snow and soil moisture storages. Variables are defined in Tables 3 and 4. Each water balance component is formulated on a daily scale.

Table 3
Snow storage water balance variables and equations, applied daily to each sub-basin (Fig. 1.b).

Variable	Dimension	Equation or data source
Effective precipitation	L/T	$P_e = m_cP + m_r$
Snowmelt coefficient	–	$m_c = \begin{cases} 0 & T < T_F \\ 1 & T > T_M \\ \frac{T - T_F}{T_M - T_F} & T_F < T < T_M \end{cases}$
Snow accumulation	L/T	$Ac_t = Ac_{t-1} + (1 - m_c)P_t$
Snow Melt	L/T	$m_r = m_cAc$
Total precipitation	L/T	P
Freezing point	°C	T_F: Calibration parameter
Melting Point	°C	T_M: Calibration parameter
Air (Observed) temperature	°C	T

Table 4
Soil moisture storage water balance variables and equations, applied daily to each sub-basin (Fig. 1.b) (Yates et al., 2005).

Variable	Dimension	Equation or data source
Storage change	L^3/T	$\frac{\Delta S_{rz}}{\Delta t} = SWC.A\frac{\Delta z}{\Delta t} = P_eA - ET_{act}A - Q_{sur} - Q_{int} - Q_r + Q_{ISW}$
Relative soil water content	–	$z_{t+1} = z_t + \Delta z$
Actual evapotranspiration	L/T	$ET_{ac} = (PET)K_c\left(\frac{5z1 - 2z^2}{3}\right)$
Surface runoff	L^3/T	$Q_{sur} = (Q_{ISW} + P_eA)z^{RRF}$
Subsurface runoff (Interflow)	L^3/T	$Q_{int} = fKz^2A$
Groundwater recharge	L^3/T	$Q_r = (1-f)Kz^2A$
Irrigation with surface water	L^3/T	Q_{ISW}
Effective precipitation	L/T	P_e (This is calculated from Table 3)
Area for each sub-basin	L^2	A
Potential Evapotranspiration	L/T	PET: Penman-Monteith method using input meteorological data from synoptic weather station (Source: Iran Meteorological Organization, see https://data.irimo.ir/)
Crop coefficient	–	K_c
Runoff resistance factor	–	RRF: Calibration parameter
Preferred flow direction	–	$f = 1 \Rightarrow Q_r = 0$ and $Q_{int} = Kz^2A$ (There is no GW in the study area (Yekom Consulting Engineers, 2016))
Root zone conductivity	L/T	K: Calibration parameter
Soil water capacity	L	SWC: Calibration parameter
Initial Relative soil water content	–	Z_1: Calibration parameter

specific groundwater aquifer in the region due to the mountainous nature of the region (Yekom Consulting Engineers, 2016), and groundwater recharge is considered zero. The observed weather data, such as precipitation, temperature, relative humidity, wind speed, and sunshine hours, were obtained from the Meteorological Organization of Iran. The required land use information was extracted from Urmia Lake Restoration Program and Food and Agriculture Organization reports. Land use includes three rainfed, rangeland, and irrigated groups in the study area (Table 5).

3.3. *Multiobjective calibration of hydrological rainfall-runoff model using MOPSO optimization algorithm*

This study used two objective functions based on NSE (Eq. 8 and Eq. 9). The multiobjective perspective can reduce the uncertainty of determining the parameters of the hydrological model compared to the single-objective calibration process (Her and Seong, 2018; Schoups et al., 2005). Determining the objective functions is one of the essential steps in developing hydrological models. In some cases, due to the low diversity of observational data, lack of soil moisture data and groundwater level, and low discharge of rivers in the basin, a unique approach should be used to determine the objective functions. Approaches such as reverse flow (Pushpalatha et al., 2012) or logarithm of flow (Oudin et al., 2006; Roodari et al., 2020) are suitable for objective functions. For this reason, the approach of maximizing the simulation accuracy of observed flow and logarithm of flow were used as calibration objective functions in the present study. The calibration of the model was done using the observed temperature and precipitation input variables. Precipitation of upstream Bukan reservoir is very low from mid-spring to mid-autumn, as inflow to the reservoir is supplied by snowmelt during these dry months. To assess any potential trade-offs in the model in fitting low and high flows, we use two objective functions that capture these two flow regimes:

Table 5
Area and vegetation categories in each sub-basin of upstream Bukan reservoir (see the location of hydrometric stations in Fig. 1) (Yekom Consulting Engineers, 2016).

Sub-basin	Hydrometric station	Crop		Orchard		Rainfed	Rangeland
		Area [km^2]	No. categories	Area [km^2]	No. categories	Area [km^2]	Area [km^2]
Saruq river	**Safakhaneh (H1)**	37	4*	39.5	5**	312.5	2013.7
Khoorkhooreh river	**Darrepanbedan (H2)**	150.8	7***	37.5	5**	218.6	1622.7
ZRR upstream	**Polesaheb (H3)**					149.8	1224.1
Saqqez river	**Qabqabloo (H4)**					239.7	858.6
Total Area [km^2]		187.8		77		920.6	5719.1

* Crops include alfalfa, barley, vegetable, and wheat.
** Orchards include apple, conifer tree, grapes, stone fruit, and walnut.
*** Crops include alfalfa, barley, bean, sugarbeet, sunflower, vegetable, and wheat.

$$\mathrm{NSE}_Q = 1 - \frac{\sum_{t=1}^{T}\left(Q_s^t - Q_o^t\right)^2}{\sum_{t=1}^{T}\left(Q_o^t - \bar{Q}_o\right)^2} \tag{8}$$

$$\mathrm{NSE}_{LogQ} = 1 - \frac{\sum_{t=1}^{T}\left(LogQ_s^t - LogQ_o^t\right)^2}{\sum_{t=1}^{T}\left(LogQ_o^t - \bar{LogQ}_o\right)^2} \tag{9}$$

where Q_s^t and Q_o^t represent the simulated and observed flow in daily time step, respectively.$\bar{Q}_o$ and $\bar{LogQ}_o$ are the average observed flow and the average logarithm of flow, respectively, over the calibration period. The output of the two-objective calibration is a Pareto front of multiple solutions, and the following Euclidean Distance (ED) formula (Eq. 10) is used to identify a single best model run (Hrachowitz and Clark, 2017).

$$\mathrm{ED} = \sqrt{\left(1 - NSE_Q\right)^2 + \left(1 - NSE_{LogQ}\right)^2} \tag{10}$$

The MOPSO algorithm was used to calibrate the two-objective hydrological model (Coello et al., 2004). Fig. 9 illustrates the step-by-step procedure of MOPSO and its interaction with the hydrological rainfall-runoff model. In MOPSO, the algorithm starts by creating a random population of x_i particles (Fig. 9b), so that each particle has an n-dimensional set for n calibration parameters. In this study, each particle is a 6-parameter set of snow and soil moisture storage calibration parameters $\{SWC, K, RRF, Z_1, T_F, T_M\}$(see Table 3 and Table 4), with upper and lower limits shown in Table 6. Each particle represents a set of calibration parameters used to run the hydrological model for the entire simulation period (2001–2014) on a daily time scale. Daily flow and logarithm flow are simulated by the hydrologic model, and they are imported to the optimization model for calculating the objective functions. The process is repeated for each particle in the current population. Finally, non-dominated particles in the population are saved and added to the Pareto set. If the stopping criterion of the optimization model is not reached, a new population of particles is generated by the optimization algorithm, and the entire procedure is repeated. Finally, the best parameters set of Pareto fronts with the minimum ED is selected for the hydrological rainfall-runoff model. More details about MOPSO and its parameters are presented in (Coello et al., 2004; Dehghanipour

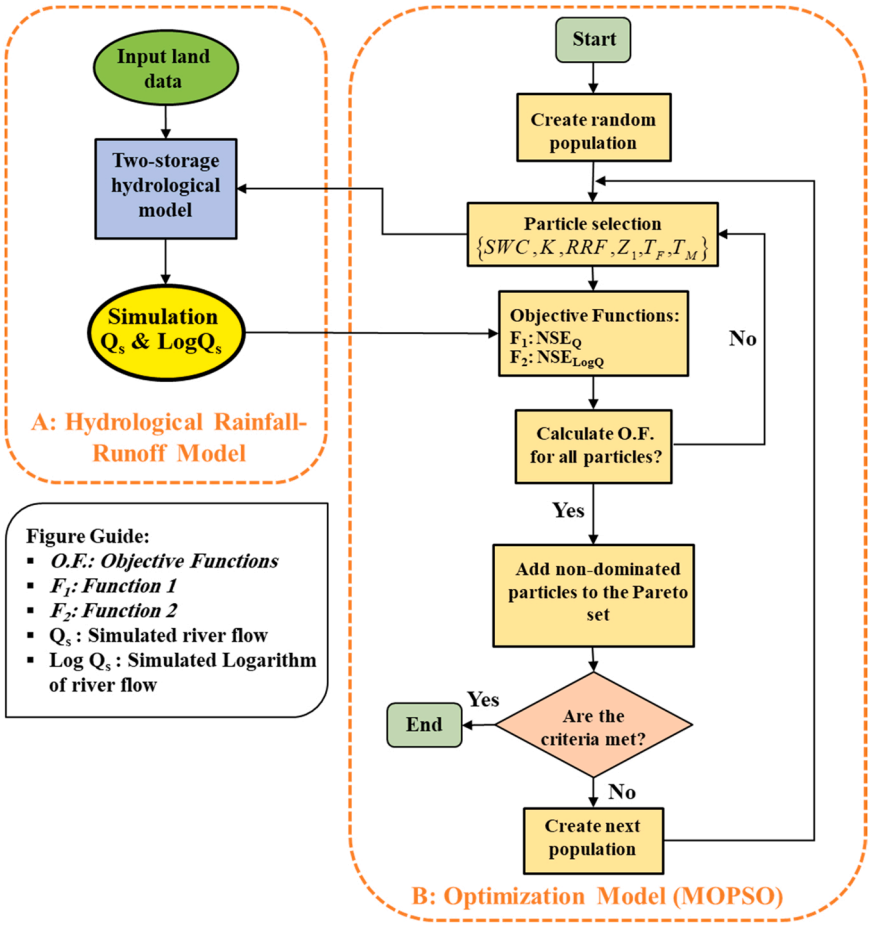

Fig. 9. Outline of calibration of hydrological rainfall-runoff model using MOPSO.

Table 6
Calibration parameters and their threshold for Hydrological Rainfall-Runoff Model. These parameters are determined for each sub-basin (Fig. 1b).

Parameter	SWC	RRF	K	Z_1	$T_{Freezing}$	$T_{Melting}$
Unit	mm	No unit	mm/day	No unit	°C	°C
Description	Soil water capacity	Runoff resistance factor	Root zone conductivity	Initial Relative soil water content	Freezing point	Melting Point
Min	50	0	0	5	-2.5	$T_{Freezing}$ Value
Max	1500	20	300	45	2.5	10

et al., 2019).

The calibration period was considered for 11 years in a daily time step (A total of 4018 time steps) for the period 2003–2014. Moreover, the period of 1999–2003 (1826 time steps) was examined as a validation period.

4. Results

4.1. Weather forecast downscaling

4.1.1. AI downscaling methods

For a better understanding of the functionality of the mentioned AI methods in downscaling weather forecasts, the efficiency of each method was examined separately. Table 7 summarizes the efficiency criteria of downscaled precipitation forecasts for Tekab and Saqez synoptic stations. The optimization results show that the hybrid approach has far better efficiency than SVR and GMDH for ECMWF and NCEP data. In this case, NSE values of the hybrid approach were twice those of the non-hybrid methods.

The results also show the better performance of the ECMWF monthly precipitation forecasts for both stations and on both test and train data. In all three optimization methods, the optimization results of ECMWF are much better than NCEP. One reason is their different approach in forecasting weather conditions. NCEP uses a hydrostatic model combined with approximate estimates of topography. ECMWF, on the other hand, uses a non-hydrostatic model and more precisely accounts for topographic effects on the weather forecast (Owens and Hewson, 2018; Saha et al., 2010). Therefore, ECMWF has better performance in mountainous areas (Sodoudi et al., 2010). Moreover, test data had higher NSE than train data as the (end of the) test data period benefits from ECMWF's new update to SEAS5 in 2017, which includes an upgraded resolution and many other features.

Table 8 shows that results of downscaling daily temperature at 2 m are similar for both NCEP and ECMWF forecasts. Downscaling temperature with the GMDH method is acceptable since the temperature is not a random phenomenon like precipitation, and there is no significant benefit in using a more complex hybrid method. The corresponding forecast time series in Fig. 10 show that the GMDH downscaling method is capable of reducing the difference between observed and raw forecast data.

4.1.2. BBN downscaling method

The BBN precipitation forecast model was used to forecast monthly precipitation. For validating the trained network, Accuracy criteria, confusion matrix (Table 9), and ROC Curve (Fig. 11) were calculated for the child (output) node. These are BBN's probabilistic results for showing its efficiency (BayesFusion, 2017). The ROC Curve for forecasting precipitation at Saqez station is shown in Fig. 11. The corresponding confusion matrix and accuracy criterion of the station are presented in Table 9 and Table 10, respectively. The values of the area under the ROC curve (AUC) for all precipitation categories are shown in Table 10. The numbers on the main diameter of the confusion matrix are more significant than the other arrays, indicating that the trained BBN simulates the true positive and the false positive with reasonable accuracy for different categories. Moreover, the Accuracy and AUC values for different categories are close to 1, indicating the BBN's acceptable performance and accuracy.

4.1.3. Comparison of BBN and hybrid AI downscaling methods

Fig. 12 shows the train and test results of precipitation downscaling methods and observed data, in which BBN method was better able to fit the diagram with observed data. Furthermore, the downscaled forecasts from the BBN and hybrid AI methods in 2020 and 2021 were compared with the observed precipitation data at Saqez station (Fig. 13 and Table 11). The probabilistic categorical

Table 7
Efficiency criteria of downscaled ECMWF and NCEP precipitation forecasts for a 1-month lead time.

		ECMWF						NCEP					
		SVR		GMDH		SVR-GMDH (Hybrid)		SVR		GMDH		SVR-GMDH (Hybrid)	
		NSE	RMSE	NSE	RMSE	NSE	RMSE	NSE	RMSE	NSE	RMSE	NSE	RMSE
Tekab station	Train data	0.27	0.08	0.16	0.34	0.54	1.00	0.24	3.54	0.18	4.50	0.33	3.59
	Test data	0.34	4.44	0.27	6.04	0.61	3.54	0.27	1.52	0.18	0.08	0.39	1.44
Saqez station	Train data	0.22	2.44	0.24	2.79	0.53	1.90	0.16	6.25	0.11	6.37	0.37	6.38
	Test data	0.37	2.68	0.54	3.4	0.62	2.43	0.28	3.79	0.31	4.28	0.41	3.76

Table 8
Efficiency criteria of downscaled ECMWF and NCEP temperature forecasts for 6-month lead time.

		GMDH			
		ECMWF		NCEP	
		NSE	RMSE	NSE	RMSE
Tekab station	Train data	0.81	0.01	0.86	0.01
	Test data	0.86	0.09	0.84	0.01
Saqez station	Train data	0.76	0.04	0.83	0.01
	Test data	0.84	0.13	0.81	0.01

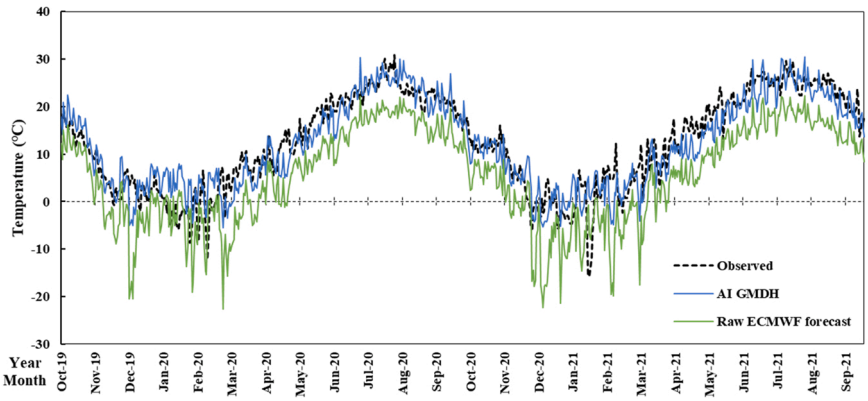

Fig. 10. Comparison of raw (ECMWF) and downscaled daily temperature forecasts at Saqez station using the GMDH downscaling method.

Table 9
Confusion matrix for downscaled precipitation at Saqez station.

		Simulated				
		S1	S2	S3	S4	S5
Observed	S1	33	0	0	0	0
	S2	7	25	1	0	0
	S3	3	4	27	0	0
	S4	0	1	2	29	1
	S5	0	2	1	5	25

forecasts from the BBN model were converted into a single-value forecast by computing the average of each precipitation category weighted by the forecast probability of each category. Fig. 13 and Table 11 show the BBN has a better performance in downscaling precipitation, and it better captures the dynamics in the observed data.

A possible reason for the better performance may be due to the probabilistic nature of the BBN in better capturing the random nature of precipitation dynamics compared to the deterministic AI methods. As discussed earlier, the deterministic methods work better for temperature, which generally has greater predictability.

4.2. Hydrological model calibration

In this study, a computer was used with a 2.8 GHz CPU and 16 GB of RAM. The running time of the hydrological rainfall-runoff model and optimization model took 35 s in the daily time step. About 30 s was dedicated to the running time of the hydrological model and about 5 s to call the results of runoff simulation, calculate the objective functions in the calibration process, and apply new calibration parameters to the hydrological model. Fig. 14 shows optimization results of the MOPSO algorithm after 7250 model runs for Saruq river sub-basin. It shows no significant trade-off between the two objective functions, and improving one objective function does not significantly affect the performance of the other objective function. This suggests that the rainfall-runoff model adequately captures both low flows (baseflow) and high flows.

However, many errors and uncertainties would occur in a single-objective calibration approach for estimating parameters. For instance, in Fig. 14, the three points A, B, and C correspond to maximum simulation accuracy of the logarithm of flow, the minimum ED, and maximum simulation accuracy of flow, respectively. Based on Fig. 14, if the one-objective calibration was applied to maximize NSE_{logQ}, the value would be 0.55 for NSE_{LogQ} (corresponding to point A). This value is slightly higher than the value corresponding to the minimum ED in a two-objective calibration of 0.54 (point B); but the NSE_Q in the single-objective calibration was 0.2 (point A),

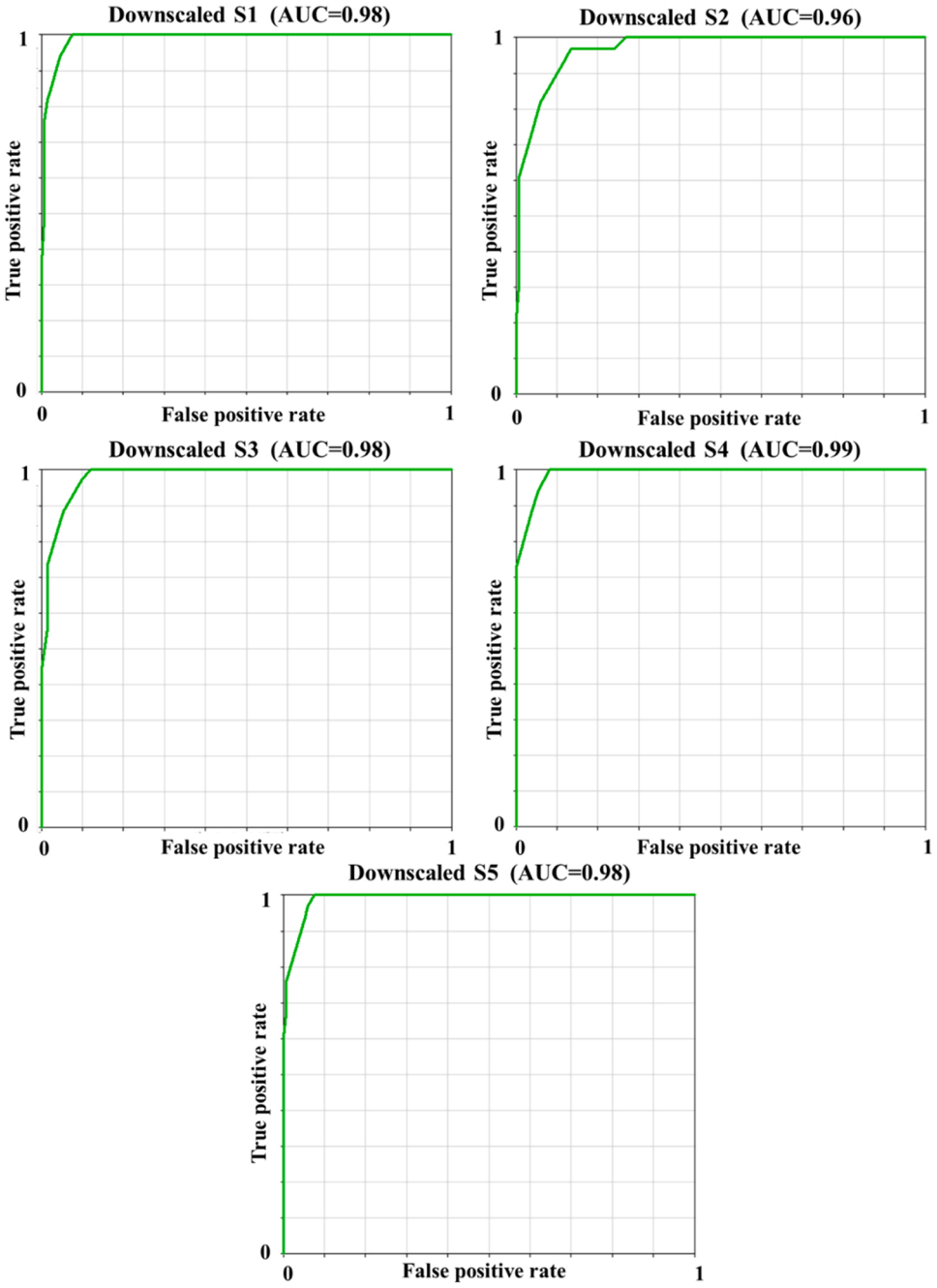

Fig. 11. ROC Curve of different categories for downscaled precipitation (Table 2).

Table 10
Accuracy and area under ROC curve for downscaled precipitation at Saqez station.

	Area under receiver operating characteristic curve (AUC)	Accuracy
S1	0.98	0.84
S2	0.96	
S3	0.98	
S4	0.99	
S5	0.98	

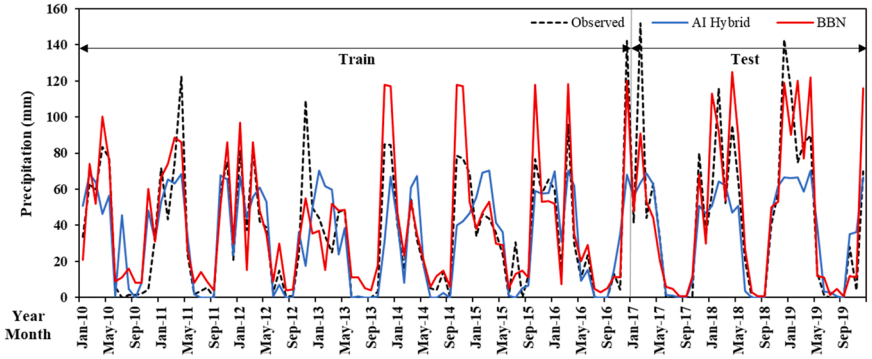

Fig. 12. Train and test results: Monthly time series of observed precipitation and 1-month forecasted precipitation by BBN and hybrid AI methods at Saqez station.

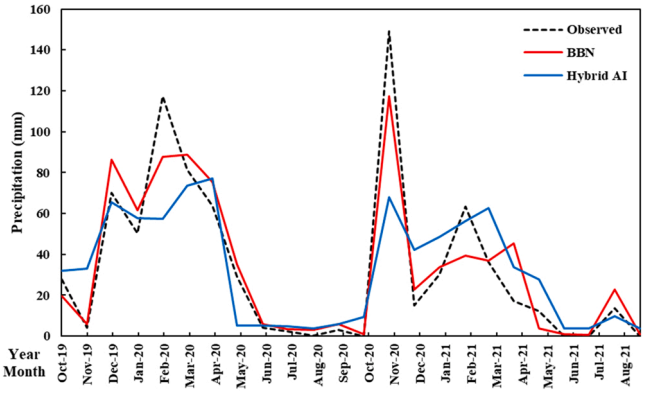

Fig. 13. Comparison of 1-month precipitation forecasts by the BBN and hybrid AI methods with observed precipitation in 2020 and 2021 at Saqez station.

Table 11
Efficiency of BBN and hybrid AI methods for 1-month precipitation forecasts in the years 2020 and 2021 at Saqez station.

	BBN	Hybrid AI
NSE	0.88	0.61
RMSE	13.24	24.54

which is very different from the value corresponding to the minimum ED in the two-objective calibration, which is equal to 0.55 (point B). Convergence of the MOPSO calibration was assessed by visual inspection of the Pareto front and the calibration was stopped when the Pareto front did not show significant changes between successive iterations.

Fig. 15 shows scatter diagrams of the objective functions versus the calibration parameters for the Saruq river sub-basin. When SWC increases, the two objective functions first increase and then decrease with an optimal value around 300 mm. The concentration of scatter points around the vertical axis in the plots for parameters K and Z_1 is evident for both objective functions, indicating that optimal values for these parameters are close to their lower limit (Table 6). Z_1 corresponds to the relative soil water content at the start of the simulation (1 October), when rainfall is low, and soils are likely dry. Likewise, the small value for parameter K reflects the mountainous nature of the region, with soils having low permeability. According to Fig. 15, values of the objective functions are highly sensitive to the parameters representing freezing and melting temperature, as would be expected in a region where runoff is affected by significant snow accumulation and snowmelt.

Optimal values of the calibration parameters in ZRR upstream, Saqez River, Saruq River, and Khoorkhooreh River sub-basins corresponding to Maximum NSE_Q, Maximum NSE_{LogQ}, and minimum ED are summarized in Table 12. The results of this Table show that the optimum freezing point (T_F) and melting point (T_M) for the snow storage of these sub-basins are close to the upper limit of these parameters in Table 6. By examining the region's data, we considered values up to 10 °C for melting parameter (T_M) since it may take until May (with average temperature of 10 °C) for snow to completely disappear. This shows the mountainous nature of the study area and snow's predominant role in the water balance equation, indicating the early freezing of precipitation in winter and the

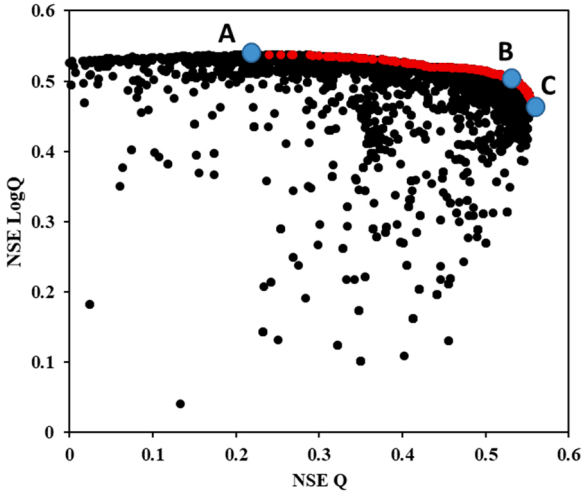

Fig. 14. Pareto plot for the multi-objective calibration after 7250 model simulations for Saruq river sub-basin with the MOPSO algorithm. Each point shows one simulation of the hydrological rainfall-runoff model, red points indicate the Pareto front, i.e. the set of non-dominated simulations.

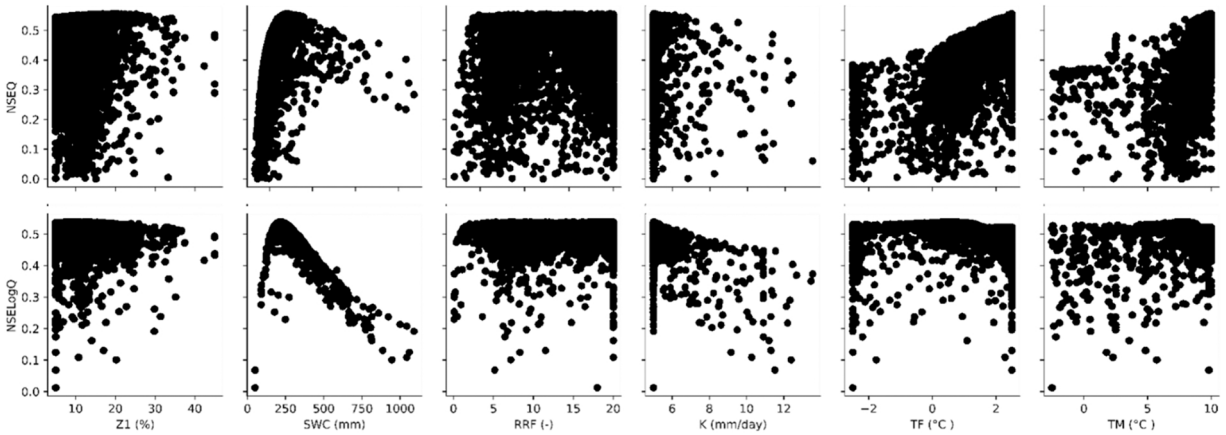

Fig. 15. Scatter plots of all calibration parameters and two objective functions for Saruq river sub-basin.

late melting of snow in spring. Furthermore, as discussed earlier, Z_1 and K are closer to their lower limits (Table 12).

Table 13 shows NSE values for simulating daily river runoff and logarithm of flow for each sub-basin during calibration and validation periods. Most NSE values in this table are above 0.5. Similar or lower NSE values (0.4–0.5) were obtained in previous simulation studies for this basin (Emami and Koch, 2019; Moriasi et al., 2007), with the critical caveat that those were based on monthly flows, whereas here we calculate the performance of daily flow simulations.

For instance, Fig. 16 shows simulated and observed time series of Saruq River flow. The NSE results of Table 13 and the comparison of simulated and observed flow in Fig. 16 show the model's acceptable performance in simulating wet and dry periods within the year as well as simulating drought and wet years.

Finally, precipitation and temperature outputs of the weather forecast downscaling model were used to force the hydrological rainfall-runoff model. Fig. 17 shows the daily forecasted inflow to Bukan reservoir by the runoff forecast system and observed inflow to Bukan reservoir in 2020 and 2021. We note that the runoff forecasting model generates accurate forecasts in both dry and wet months, with an overall NSE value of 0.66 for two consecutive years. Forecast performance is better in wet months. This time period is important because there is a possibility of floods at this time and because it is a non-agricultural season during which optimal management of the reservoir could maximize surplus water allocations for meeting the environmental needs of UL. The model was also able to forecast days of peak inflow on March 18th and April 8th 2020, and March 15th 2021; forecasting these days is essential from two perspectives. First, it can lead to better flood management and thereby reduce downstream damages. Second, forecasting the volume of water inflow to the reservoir can help in the optimal cultivation planning so that in case of drought, financial losses will not be inflicted on farmers.

Table 12
Calibrated parameter values corresponding NSE values for the calibration period.

Sub-basin	Parameter	Maximum NSE_Q	Maximum NSE_{LogQ}	Minimum Euclidean distance
Saruq river	SWC [mm]	354.1	219.4	310.8
	RRF	17.5	8.9	17
	K [mm/day]	5	5	5
	Z_1	20.5	8.6	16.3
	T_F [°C]	2.5	0.5	2.5
	T_M [°C]	10	7.7	10
Khoorkhooreh river	SWC [mm]	606.9	450.5	504.4
	RRF	5.1	2.8	5.7
	K [mm/day]	5	5	5
	Z_1	14	8.4	10.1
	T_F [°C]	2.2	2.4	2.1
	T_M [°C]	3.8	3.6	3.4
ZRR upstream	SWC [mm]	1234.1	195.2	242.5
	RRF	20	16.1	20
	K [mm/day]	300	6	12.5
	Z_1	5	5	7.6
	T_F [°C]	2.5	2.5	2.5
	T_M [°C]	10	9.4	10
Saqqez river	SWC [mm]	1006.9	180.3	224.5
	RRF	15.9	19.3	5.5
	K [mm/day]	300	5	12.8
	Z_1	5.6	21.1	18.7
	T_F [°C]	2.5	2.5	2.5
	T_M [°C]	10	9.9	10

Table 13
NSE values for calibration and validation periods.

	Calibration period		Validation period	
Sub-basin	**NSE_Q**	**NSE_{LogQ}**	**NSE_Q**	**NSE_{LogQ}**
Saruq river	0.55	0.54	0.60	0.46
Khoorkhooreh	0.45	0.71	0.64	0.78
ZRR upstream	0.33	0.64	0.50	0.51
Saqez river	0.38	0.64	0.43	0.54
Average	**0.43**	**0.63**	**0.54**	**0.57**

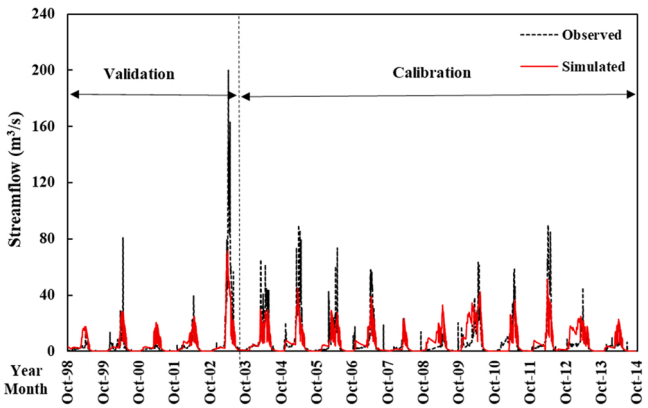

Fig. 16. Daily time series of observed and simulated stream flow of Saruq river hydrometric station.

5. Conclusion

This study developed and applied the first runoff forecast system on a daily time scale for upstream inflow into Bukan reservoir, a key component of the water management infrastructure in ULB. The forecast system consists of two models: (1) a weather forecast model that downscales the large-scale weather outputs of ECMWF and NCEP to small-scale spatial resolutions and (2) a hydrological rainfall-runoff model that forecasts inflow into Bukan reservoir. The weather forecast downscaling model was developed based on two probabilistic and deterministic approaches and produced temperature and precipitation inputs for the hydrological rainfall-runoff

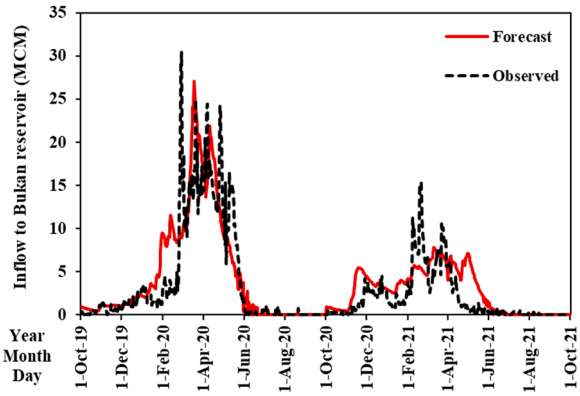

Fig. 17. Daily time series of observed and forecasted inflow to Bukan reservoir. The forecasts are made at start of each month with a 1-month lead time.

model. Three deterministic AI methods, including GMDH, SVR, and a hybrid GMDH-SVR method, as well as a probabilistic BBN, were used to downscale the raw precipitation forecasts, while GMDH was used to downscale the raw temperature forecasts. The hydrological rainfall-runoff model includes two storages: (1) snow storage that simulates daily snow accumulation and snowmelt, and (2) soil moisture storage that simulates daily water balance components in the root zone. Calibration of the hydrological model was performed using the MOPSO multi-objective optimization algorithm to estimate hydrological model parameters for each sub-basin upstream of Bukan reservoir. There is no aquifer in the study area.

The weather forecast downscaling model results show that the hybrid method performs much better than the non-hybrid methods for downscaling precipitation. Moreover, ECMWF's precipitation forecast data are more accurate than NCEP for this region. The average NSE of the hybrid method for ECMWF's 1-month lead time forecast downscaled to individual rain gauges was 0.53 and 0.62 for train and test data, respectively. By comparing the forecast precipitation of BBN and the hybrid AI method, BBN has better performance due to its probabilistic feature that helps forecast precipitation with high uncertainty. For instance, the NSE of BBN and hybrid AI for forecasting monthly precipitation were 0.88 and 0.61, respectively, in 2020 and 2021. Temperature forecast data of both organizations, ECMWF and NCEP, had acceptable accuracy and similar performance. The average NSE for train and test data, respectively, were 0.79 and 0.85 for ECMWF and 0.85 and 0.83 for NCEP forecasts with a 6-month lead time.

The calibration of the hydrological rainfall-runoff model indicates that there is no significant trade-off between maximizing objective functions for low and high flows, and improving one objective function does not deteriorate the performance of the other one. In addition, the results show that two-objective calibration reduces the uncertainty in estimating the calibration parameters compared to single-objective calibration. The average NSE in the calibration period was 0.43 and 0.63, and in the validation period, 0.54 and 0.55, respectively, for flow and logarithm of flow. Furthermore, the runoff forecast system resulted in daily forecasts of inflow into Bukan reservoir with an NSE of 0.67 in 2020 and 2021.

We conclude that the runoff forecast system developed in this study has high accuracy in forecasting inflow into Bukan reservoir. Policymakers and operators of the reservoir can use the system to forecast inflows to Bukan reservoir and optimize water allocation between agricultural and environmental demands. Moreover, this system could be beneficial to trigger prior managerial planning and actions before severe droughts or floods happen. The system used in this research can be implemented on other sub-basins and reservoirs in ULB to aid runoff forecasting and optimal management of water resources.

CRediT authorship contribution statement

Amirreza Meydani: Conceptualization, Methodology, Software, Data Curation, Visualization, Writing - Original draft, **Amirhossein Dehghanipour:** Conceptualization, Methodology, Software, Formal Analysis, Writing - Review and Editing, **Gerrit Schoups:** Conceptualization, Methodology, Validation, Investigation, Writing - Review and Editing, **Masoud Tajrishy:** Resources, Writing - Review and Editing, Investigation, Supervision.

Declaration of Competing Interest

The authors declare that they have no known competing financial interests or personal relationships that could have appeared to influence the work reported in this paper.

Data availability

Data will be made available on request.

Appendix A. Supporting information

Supplementary data associated with this article can be found in the online version at doi:10.1016/j.ejrh.2022.101228.

References

[dataset] ECMWF, 2021a. Seasonal forecast monthly statistics on single levels [WWW Document]. https://doi.org/10.24381/cds.68dd14c3.

[dataset] ECMWF, 2021b. Seasonal forecast daily and subdaily data on single levels [WWW Document]. https://doi.org/10.24381/cds.181d637e.

[dataset] NCEP, 2011. CFSv2 Operational Forecasts Time Series [WWW Document]. URL ⟨https://www.ncei.noaa.gov/products/weather-climate-models/climate-forecast-system⟩.

Adamowski, J., 2013. Using support vector regression to predict direct runoff, base flow and total flow in a mountainous watershed with limited data in Uttaranchal, India. Ann. Warsaw Univ. Life Sci. - SGGW. L. Reclam. 45, 71–83. https://doi.org/10.2478/sggw-2013–0007.

Ahmadaali, J., Barani, G.-A., Qaderi, K., Hessari, B., 2017. Calibration and validation of model WEAP21 for Zarrineh Rud and Simineh Rud basins. Iran. J. Soil Water Res. 48, 823–839. https://doi.org/10.22059/ijswr.2017.216989.667543.

Ahmadi, A., Nasseri, M., Solomatine, D.P., 2019. Parametric uncertainty assessment of hydrological models: coupling UNEEC-P and a fuzzy general regression neural network. Hydrol. Sci. J. 64, 1080–1094. https://doi.org/10.1080/02626667.2019.1610565.

Arpe, K., Leroy, S.A.G., Wetterhall, F., Khan, V., Hagemann, S., Lahijani, H., 2014. Prediction of the Caspian Sea level using ECMWF seasonal forecasts and reanalysis. Theor. Appl. Climatol. 117, 41–60. https://doi.org/10.1007/s00704-013-0937-6.

BayesFusion, L. L. C. (2017). GeNIe Modeler. *User Manual. Available online: https://support.bayesfusion.com/docs/(accessed on 21 October 2019)*.

Benderskaya, E.N., 2013. Nonlinear Trends in Modern Artificial Intelligence: A New Perspective. In: Kelemen, J., Romportl, J., Zackova, E. (Eds.), Beyond Artificial Intelligence. Topics in Intelligent Engineering and Informatics, 4. Springer, Berlin, Heidelberg. 10.1007/978-3-642-34422-0_8.

Chen, Y., Sharma, S., Zhou, X., Yang, K., Li, X., Niu, X., Hu, X., Khadka, N., 2021. Spatial performance of multiple reanalysis precipitation datasets on the southern slope of central Himalaya. Atmos. Res. 250, 105365 https://doi.org/10.1016/j.atmosres.2020.105365.

Chevalier, R.F., Hoogenboom, G., McClendon, R.W., Paz, J.A., 2011. Support vector regression with reduced training sets for air temperature prediction: a comparison with artificial neural networks. Neural Comput. Appl. 20, 151–159. https://doi.org/10.1007/s00521-010-0363-y.

Coello, C.A.C., Pulido, G.T., Lechuga, M.S., 2004. Handling multiple objectives with particle swarm optimization. IEEE Trans. Evol. Comput. 8, 256–279. https://doi.org/10.1002/9780470612163.

Dariane, A.B., Pouryafar, E., 2021. Quantifying and projection of the relative impacts of climate change and direct human activities on streamflow fluctuations. Clim. Change 165, 34. https://doi.org/10.1007/s10584-021-03060-w.

Dehghanipour, A.H., Zahabiyoun, B., Schoups, G., Babazadeh, H., 2019. A WEAP-MODFLOW surface water-groundwater model for the irrigated Miyandoab plain, Urmia lake basin, Iran: multi-objective calibration and quantification of historical drought impacts. Agric. Water Manag. 223, 105704 https://doi.org/10.1016/j.agwat.2019.105704.

Dehghanipour, A.H., Schoups, G., Zahabiyoun, B., Babazadeh, H., 2020. Meeting agricultural and environmental water demand in endorheic irrigated river basins: a simulation-optimization approach applied to the Urmia Lake basin in Iran. Agric. Water Manag. 241, 106353 https://doi.org/10.1016/j.agwat.2020.106353.

Dehghanipour, M.H., Karami, H., Ghazvinian, H., Kalantari, Z., Dehghanipour, A.H., 2021. Two comprehensive and practical methods for simulating pan evaporation under different climatic conditions in Iran. Water 13, 2814. https://doi.org/10.3390/w13202814.

Dodangeh, E., Panahi, M., Rezaie, F., Lee, S., Tien, D., 2020. Novel hybrid intelligence models for flood-susceptibility prediction: meta optimization of the GMDH and SVR models with the genetic algorithm and harmony search. J. Hydrol. 590, 125423 https://doi.org/10.1016/j.jhydrol.2020.125423.

Dunn, S.M., Stalham, M., Chalmers, N., Crabtree, B., 2003. Adjusting irrigation abstraction to minimise the impact on stream flow in the east of Scotland. J. Environ. Manag. 68, 95–107. https://doi.org/10.1016/S0301-4797(03)00006-9.

ECMWF, 2013. IFS documentation – Cy38r1, Part III: Dynamics and numerical procedures Table of contents. Shinfield Park, Reading, RG2 9AX, England.

Emami, F., Koch, M., 2019. Modeling the impact of climate change on water availability in the Zarrine River basin and inflow to the Boukan Dam, Iran. Climate 7. https://doi.org/10.3390/cli7040051.

Fawcett, T., 2006. An introduction to ROC analysis. Pattern Recognit. Lett. 27, 861–874. https://doi.org/10.1016/j.patrec.2005.10.010.

Ficchì, A., Raso, L., Dorchies, D., Pianosi, F., Malaterre, P.-O., Van Overloop, P.-J., Jay-Allemand, M., 2016. Optimal operation of the multireservoir system in the Seine River basin using deterministic and ensemble forecasts. J. Water Resour. Plan. Manag. 142, 05015005 (10.1061/(asce)wr.1943-5452.0000571).

Gavahi, K., Mousavi, S.J., Ponnambalam, K., 2019. Adaptive forecast-based real-time optimal reservoir operations: application to Lake Urmia. J. Hydroinformatics 21, 908–924. https://doi.org/10.2166/hydro.2019.005.

Geng, J., Gan, W., Xu, J., Yang, R., Wang, S., 2020. Support vector machine regression (SVR)-based nonlinear modeling of radiometric transforming relation for the coarse-resolution data-referenced relative radiometric normalization (RRN). Geo-Spat. Inf. Sci. 23, 237–247. https://doi.org/10.1080/10095020.2020.1785958.

Ghaheri, M., Baghal-Vayjooee, M.H., Naziri, J., 1999. Lake Urmia, Iran: a summary review. Int. J. Salt Lake Res. 8, 19–22. https://doi.org/10.1007/bf02442134.

Goodarzi, L., Banihabib, M.E., Roozbahani, A., Dietrich, J., 2019. Bayesian network model for flood forecasting based on atmospheric ensemble forecasts. Nat. Hazards Earth Syst. Sci. 19, 2513–2524. https://doi.org/10.5194/nhess-19-2513-2019.

Govender, I.H., Sahlin, U., O'Brien, G.C., 2021. Bayesian network applications for sustainable holistic water resources management: modeling opportunities for South Africa. Risk Anal. 0, risa.13798 https://doi.org/10.1111/risa.13798.

Grillakis, M., Koutroulis, A., Tsanis, I., 2018. Improving seasonal forecasts for basin scale hydrological applications. Water 10, 1593. https://doi.org/10.3390/w10111593.

Gubler, S., Sedlmeier, K., Bhend, J., Avalos, G., Coelho, C.A.S., Escajadillo, Y., Jacques-Coper, M., Martinez, R., Schwierz, C., de Skansi, M., Spirig, C., 2020. Assessment of ECMWF SEAS5 seasonal forecast performance over South America. Weather Forecast 35, 561–584. https://doi.org/10.1175/WAF-D-19-0106.1.

Her, Y., Seong, C., 2018. Responses of hydrological model equifinality, uncertainty, and performance to multi-objective parameter calibration. J. Hydroinformatics 20, 864–885. https://doi.org/10.2166/hydro.2018.108.

Hrachowitz, M., Clark, M.P., 2017. HESS Opinions: The complementary merits of competing modelling philosophies in hydrology 3953–3973.

Hruschka, E.R., Nicoletti, M., do, C., 2013. Roles played by Bayesian networks in machine learning: an empirical investigation. Smart Innov. Syst. Technol. 13, 75–116. https://doi.org/10.1007/978-3-642-28699-5_5.

Ivakhnenko, A.G., 1970. Heuristic self-organization in problems of engineering cybernetics. Automatica 6, 207–219. https://doi.org/10.1016/0005-1098(70)90092-0.

Johnson, S.J., Stockdale, T.N., Ferranti, L., Balmaseda, M.A., Molteni, F., Magnusson, L., Tietsche, S., Decremer, D., Weisheimer, A., Balsamo, G., Keeley, S.P.E., Mogensen, K., Zuo, H., Monge-sanz, B.M., Park, S., 2019. SEAS5: the new ECMWF seasonal forecast system 1087–1117.

Kaune, A., Chowdhury, F., Werner, M., Bennett, J., 2020. The benefit of using an ensemble of seasonal streamflow forecasts in water allocation decisions. Hydrol. Earth Syst. Sci. 24, 3851–3870. https://doi.org/10.5194/hess-24-3851-2020.

Khan, M.S., Coulibaly, P., 2006. Bayesian neural network for rainfall-runoff modeling. Water Resour. Res. 42, 1–18. https://doi.org/10.1029/2005WR003971.

Khorasani, H., Kerachian, R., Malakpour-Estalaki, S., 2018. Developing a comprehensive framework for eutrophication management in off-stream artificial lakes. Journal of Hydrology 562, 103–124. https://doi.org/10.1016/j.jhydrol.2018.04.052.

Kisi, O., Cimen, M., 2012. Precipitation forecasting by using wavelet-support vector machine conjunction model. Eng. Appl. Artif. Intell. 25, 783–792. https://doi.org/10.1016/j.engappai.2011.11.003.

Lang, Y., Luo, L., Ye, A., Duan, Q., 2020. Do CFSv2 seasonal forecasts help improve the forecast of meteorological drought 1–14. ⟨https://doi.org/10.3390/w12072010⟩.
Liu, Y., Wang, H., Lei, X., Wang, H., 2021. Real-time forecasting of river water level in urban based on radar rainfall: a case study in Fuzhou City. J. Hydrol. 603, 126820 https://doi.org/10.1016/j.jhydrol.2021.126820.
Mahmudi, P., Motamedvaziri, B., Hosseini, M., Ahmadi, H., Amini, A., 2021. Study of climate change effects on hydrological processes in Siminehroud and Zarrinehroud watersheds northwest of Iran Study of climate change effects on hydrological processes in Siminehroud and Zarrinehroud watersheds northwest of Iran. ⟨https://doi.org/10.1007/s12145–021-00598–2⟩.
Mancosu, N., Snyder, R.L., Kyriakakis, G., Spano, D., 2015. Water scarcity and future challenges for food production. Water 7, 975–992. https://doi.org/10.3390/w7030975.
Meydani, A., Dehghanipour, A., Tajrishy, M., 2021. Development of a daily rainfall-runoff model to simulate the Bukan reservoir inflow and quantify the effects of severe historical drought using WEAP model and multiobjective calibration. Iran. -Water Resour. Res. 17, 149–164.
Molina, J.L., Pulido-Velázquez, D., García-Aróstegui, J.L., Pulido-Velázquez, M., 2013. Dynamic Bayesian networks as a decision support tool for assessing climate change impacts on highly stressed groundwater systems. J. Hydrol. 479, 113–129. https://doi.org/10.1016/j.jhydrol.2012.11.038.
Moriasi, D.N., Arnold, J.G., Liew, M.W., Van, Bingner, R.L., Harmel, R.D., Veith, T.L., 2007. Model evaluation guidlines for systematic quantification of accuracy in watershed simulations. Trans. ASABE 50, 885–900.
Mostafazade, M., Alizadeh, H., 2020. Calibration of a water resource planning model using many-objective optimization. Iran. -Water Resour. Res. 15, 200–213.
Munoz, P., Munoz, D.F., Orellana-Alvear, J., Moftakhari, H., Moradkhani, H., Celleri, R., 2021. Long short-term memory networks for real-time runoff forecasting using remotely sensed data, in: EGU General Assembly. pp. 19–30. ⟨https://doi.org/10.5194/egusphere-egu21–13900⟩, 2021.
Nariman-zadeh, N., Darvizeh, A., Darvizeh, M., Gharababaei, H., 2002. Modelling of explosive cutting process of plates using GMDH-type neural network and singular value decompositio. J. Mater. Process. Technol 128, 80–87. https://doi.org/10.1016/S0924-0136(02)00264-9.
Oudin, L., Andréassian, V., Mathevet, T., Perrin, C., Michel, C., 2006. Dynamic averaging of rainfall-runoff model simulations from complementary model parameterizations. Water Resour. Res. 42, 1–10. https://doi.org/10.1029/2005WR004636.
Owens, R., Hewson, T., 2018. ECMWF Forecast User Guide. https://doi.org/10.21957/m1cs7h.
Phan, T.D., Smart, J.C.R., Capon, S.J., Hadwen, W.L., Sahin, O., 2016. Applications of Bayesian belief networks in water resource management: a systematic review. Environ. Model. Softw. 85, 98–111. https://doi.org/10.1016/j.envsoft.2016.08.006.
Phan-Van, T., Nguyen-Xuan, T., Van Nguyen, H., Laux, P., Pham-Thanh, H., Ngo-Duc, T., 2018. Evaluation of the NCEP climate forecast system and its downscaling for seasonal rainfall prediction over Vietnam. Weather Forecast 33, 615–640. https://doi.org/10.1175/WAF-D-17-0098.1.
Pushpalatha, R., Perrin, C., Le, N., Andréassian, V., 2012. A review of efficiency criteria suitable for evaluating low-flow simulations. J. Hydrol. 420–421, 171–182. https://doi.org/10.1016/j.jhydrol.2011.11.055.
Rayner, S., Lach, D., Ingram, H., 2005. Weather forecasts are for wimps: why water resource managers do not use climate forecasts. Clim. Change 69, 197–227. https://doi.org/10.1007/s10584-005-3148-z.
Roodari, A., Hrachowitz, M., Hassanpour, F., Yaghoobzadeh, M., 2020. Signatures of human intervention – or not? Downstream intensification of hydrological drought along a large Central Asian River: the individual roles of climate variability and land use change. Hydrol. Earth Syst. Sci. Discuss. 1–40. https://doi.org/10.5194/hess-2020-369.
Saha, S., Moorthi, S., Pan, H.L., Wu, X., Wang, Jiande, Nadiga, S., Tripp, P., Kistler, R., Woollen, J., Behringer, D., Liu, H., Stokes, D., Grumbine, R., Gayno, G., Wang, Jun, Hou, Y.T., Chuang, H.Y., Juang, H.M.H., Sela, J., Iredell, M., Treadon, R., Kleist, D., Van Delst, P., Keyser, D., Derber, J., Ek, M., Meng, J., Wei, H., Yang, R., Lord, S., Van Den Dool, H., Kumar, A., Wang, W., Long, C., Chelliah, M., Xue, Y., Huang, B., Schemm, J.K., Ebisuzaki, W., Lin, R., Xie, P., Chen, M., Zhou, S., Higgins, W., Zou, C.Z., Liu, Q., Chen, Y., Han, Y., Cucurull, L., Reynolds, R.W., Rutledge, G., Goldberg, M., 2010. The NCEP climate forecast system reanalysis. Bull. Am. Meteorol. Soc. 91, 1015–1057. https://doi.org/10.1175/2010BAMS3001.1.
Saha, S., Moorthi, S., Wu, X., Wang, J., Nadiga, S., Tripp, P., Behringer, D., Hou, Y.T., Chuang, H.Y., Iredell, M., Ek, M., Meng, J., Yang, R., Mendez, M.P., Van Den Dool, H., Zhang, Q., Wang, W., Chen, M., Becker, E., 2014. The NCEP climate forecast system version 2. J. Clim. 27, 2185–2208. https://doi.org/10.1175/JCLI-D-12-00823.1.
Sangelantoni, L., Ferretti, R., Redaelli, G., 2019. Toward a regional-scale seasonal climate prediction system over central Italy based on dynamical downscaling. Climate 7. https://doi.org/10.3390/cli7100120.
Schoups, G., Addams, C.L., Gorelick, S.M., 2005. Multi-objective calibration of a surface water-groundwater flow model in an irrigated agricultural region: Yaqui Valley, Sonora, Mexico. Hydrol. Earth Syst. Sci. 9, 549–568. https://doi.org/10.5194/hess-9-549-2005.
Siegmund, J., Bliefernicht, J., Laux, P., Kunstmann, H., 2015. Toward a seasonal precipitation prediction system for West Africa: performance of CFSv2 and high-resolution dynamical downscaling. J. Geophys. Res. 120, 7316–7339. https://doi.org/10.1002/2014JD022692.
Sisto, N.P., 2009. Environmental flows for rivers and economic compensation for irrigators. J. Environ. Manag. 90, 1236–1240. https://doi.org/10.1016/j.jenvman.2008.06.005.
Sodoudi, S., Noorian, A., Geb, M., Reimer, E., 2010. Daily precipitation forecast of ECMWF verified over Iran. Theor. Appl. Climatol. 99, 39–51. https://doi.org/10.1007/s00704-009-0118-9.
Sun, L., Lan, Y., 2021. Statistical downscaling of daily temperature and precipitation over China using deep learning neural models: localization and comparison with other methods. Int. J. Climatol. 41, 1128–1147. https://doi.org/10.1002/joc.6769.
Sun, S., Leonhardt, G., Sandoval, S., Bertrand-Krajewski, J.L., Rauch, W., 2017. A Bayesian method for missing rainfall estimation using a conceptual rainfall–runoff model. Hydrol. Sci. J. 62, 2456–2468. https://doi.org/10.1080/02626667.2017.1390317.
Valipour, M., Ziatabar Ahmadi, M., Raeini-Sarjaz, M., Gholami Sefidkouhi, M.A., Shahnazari, A., Fazlola, R., Darzi-Naftchali, A., 2015. Agricultural water management in the world during past half century. Arch. Agron. Soil Sci. 61, 657–678. https://doi.org/10.1080/03650340.2014.944903.
Valverde Ramírez, M.C., Ferreira, N.J., de Campos Velho, H.F., 2006. Linear and nonlinear statistical downscaling for rainfall forecasting over southeastern Brazil. Weather Forecast 21, 969–989. https://doi.org/10.1175/WAF981.1.
Voisin, N., Pappenberger, F., Lettenmaier, D.P., Buizza, R., Schaake, J.C., 2011. Application of a medium-range global hydrologic probabilistic forecast scheme to the Ohio River basin. Weather Forecast 26, 425–446. https://doi.org/10.1175/WAF-D-10-05032.1.
Wang, F., Wang, L., Zhou, H., Valeriano, O.C.S., Koike, T., Li, W., 2012. Ensemble hydrological prediction-based real-time optimization of a multiobjective reservoir during flood season in a semiarid basin with global numerical weather predictions. Water Resour. Res. 48, 1–21. https://doi.org/10.1029/2011WR011366.
Xue, J., Gui, D., Lei, J., Sun, H., Zeng, F., Feng, X., 2017. A hybrid Bayesian network approach for trade-offs between environmental flows and agricultural water using dynamic discretization. Adv. Water Resour. 110, 445–458. https://doi.org/10.1016/j.advwatres.2016.10.022.
Yaghoubi, B., Hosseini, S.A., Nazif, S., 2019. Monthly prediction of streamflow using data-driven models. J. Earth. Syst. Sci. 128, 141 https://doi.org/10.1007/s12040-019-1170-1.
Yates, D., Sieber, J., Purkey, D., Huber-Lee, A., 2005. WEAP21 – a demand-, priority-, and preference-driven water planning model: part 1: model characteristics. Water Int. 30, 487–500. https://doi.org/10.1080/02508060508691893.
Yekom Consulting Engineers, 2016. Implementing solutions to reduce the agricultural water consumption of the Zarrinehrood and Siminehrood sub-basin by 40% (In Persian).
Yuan, X., Wood, E.F., Roundy, J.K., Pan, M., 2013. CFSv2-based seasonal hydroclimatic forecasts over the conterminous United States. J. Clim. 26, 4828–4847. https://doi.org/10.1175/JCLI-D-12-00683.1.